THE JOURNAL OF PHYSICAL CHEMISTRY B

Article

pubs.acs.org/JPCB

Exploring the Conformational Variability in the Heme b Propionic Acid Side Chains through the Effect of a Biological Probe: A Study of the Isolated Ions

Alberto De Petris,[§] Barbara Chiavarino,[§] Maria Elisa Crestoni,[§] Cecilia Coletti,[‡] Nazzareno Re,[‡] and Simonetta Fornarini*[,§]

[§]Dipartimento di Chimica e Tecnologie del Farmaco, Università degli Studi di Roma La Sapienza, P.le A. Moro 5, I-00185, Roma, Italy

[‡]Dipartimento di Farmacia, Università G. D'Annunzio, Via dei Vestini 31, I-66100 Chieti, Italy

Supporting Information

ABSTRACT: The iron(III) protoporphyrin IX complex with imidazole, a biologically relevant ligand, occupying an axial position, has been studied by infrared multiple photon dissociation (IRMPD) spectroscopy. The complex has been delivered in gas-phase by electrospray ionization (ESI), mass selected in an ion trap, and assayed by IRMPD spectroscopy in two complementary frequency regions. The fingerprint range (900−1900 cm^{-1}) has been scanned using the Orsay free-electron laser beamline (CLIO), while the X−H (X = C,N,O) stretching region (3000−3600 cm^{-1}) has been inspected using a tabletop IR optical parametric oscillator/amplifier (OPO/OPA) laser source. DFT calculations have been performed to obtain a comprehensive pattern of the various potential conformers yielding optimized geometries, relative thermodynamic parameters, and respective IR spectra. The comparison between the IR spectra for representative conformers and the experimental IRMPD features suggests the coexistence of two families of conformers involving different degrees of folding and hydrogen bonding between the two propionic acid functionalities on the periphery of the protoporphyrin IX macrocycle in a ratio depending on environmental conditions such as ESI solvent and temperature. The observed conformational variability of the porphyrin substituents in the naked heme−imidazole complex is consistent with the fine-tuning of the reactivity properties of this important prosthetic group by the specific surroundings in the protein core.

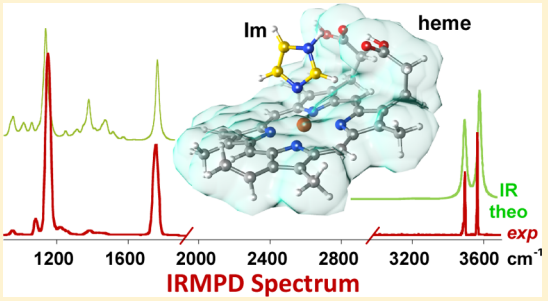

1. INTRODUCTION

The heme prosthetic group is at the core of a variety of enzymes performing key biological functions,[1−5] such as metabolic reactions of endogenous compounds or detoxification of xenobiotics, both in humans and in many other organisms. The iron center in heme b is typically six coordinate with a square bipyramidal geometry. The coordination in the plane involves four pyrrole nitrogens belonging to the protoporphyrin IX macrocycle, while other ligands, such as functional groups from the side chain of histidine or cysteine residues, a solvent molecule, a substrate or drug, can occupy the axial positions. The heme surroundings are responsible for a wide range of interactions holding the group in the protein cavity and tuning its properties. Heme−protein interactions include electrostatic attraction/repulsion, hydrogen bonding, hydrophobic stabilization, and $\pi-\pi$ stacking. The peripheral substituents on the protoporphyrin IX frame include four methyl, two vinyl, and two propionic acid (PrA) groups. The heme peripheral groups and their surroundings can modulate the electronic density on the heme iron, which in turn can modify the redox properties of the enzymes. In this context, a spectroscopic study has been undertaken combined with theoretical calculations on the electronic structural features of the complete heme, rather than the iron porphine complex that is typically used as a simpler model. The PrA groups are placed on the same "side" of the tetrapyrrole macrocyclic ligand and may exist either in the deprotonated form at physiological pH or in the neutral form in the gas-phase. For instance, from a survey of the crystallographic data on the Lanosterol 14 α-demethylase crystal structures, named CYP51, a heme enzyme, the conformations of PrAs appear to be independent of the nature of axial ligands. In general, the conformations of the PrA groups fall in two families. An exemplary typical CYP51 active site structure is characterized by both PrA groups stretched away on the porphyrin plane (Figure 1a). Alternatively, one PrA side chain is approximately perpendicular to the plane (Figure 1b). The conformational features of the naked heme, reflecting the interactions involving exclusively the porphyrin peripheral substituents, can be ascertained only when the complex is devoid of external influences. This condition may be

Received: November 12, 2014
Revised: January 8, 2015
Published: January 9, 2015

DOI: 10.1021/jp5113476
J. Phys. Chem. B 2015, 119, 1919−1929

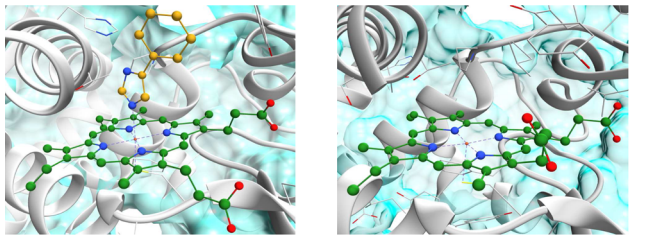

a) b)

Figure 1. An image of the active site region of the crystal structures of CYP51 complexed with 1-[3-(4-chloro-3,5-dimethylphenoxy)benzyl]-1*H*-imidazole as axial ligand (PDB ID: 4H6O) (a) or in a ligand free state (PDB ID: 2WKU) (b).

approached in an apolar solvent.[6] However, an ideal medium in this respect is the gas-phase, whereby the intrinsic properties of the heme group are least perturbed. This environment may bear, however, some affinity with the interior of a protein where the relative dielectric constant value may be as low as 2.5.[7,8] In the absence of environmental constraints, it is expected that the heme complex may sample various conformations finally presenting a thermally averaged population. In the present study, the four coordinate heme complex holding iron(III) is examined as positively charged species with the dianionic protoporphyrin IX ligand and neutral PrA groups. The Fe(III) protoporphyrin IX complex, henceforth indicated as $[FePPIX]^+$, binds an imidazole (Im) ligand, occupying an axial site and giving the complex named $[FePPIX(Im)]^+$.[9] An imidazole ligand is frequently involved from proximal histidine residues and as a key chemical functionality in substrates and drugs, including, for example, antifungal azole drugs. Computations on the $[FePPIX(Im)]^+$ complex were based on density functional theory (DFT), offering a method that is suitable to describe iron porphyrin complexes and related compounds.[10−12] In particular, the B3LYP hybrid functional has been found to perform well in providing thermodynamic data about related systems.[13,14]

Electrospray ionization (ESI)−mass spectrometry (MS) has afforded an entry to the study of charged heme complexes in the gas-phase yielding thermodynamic and kinetic parameters for the association of simple biomolecules,[15−19] relative binding energies of antimalarial agents,[20] and information about the structure of heme complexes with small peptides.[21] Insight into the conformational shape of naked $[FePPIX]^+$ has been obtained by ion mobility experiments in helium at 298 K,[22] revealing the presence of compact conformations where the PrA groups interact with each other by hydrogen bonding. The gas-phase conformation has a direct bearing on the vibrational modes of the ion, particularly the ones involved in hydrogen bond interactions. Vibrational spectroscopy of gaseous ions selected and stored in the cell of a mass spectrometer can be performed using a source of intense and tunable IR light. The ensuing "action" spectroscopy reveals the IR active modes through the absorption of multiple photons causing fragmentation of the sampled ion.[23−29] In the $[FePPIX(Im)]^+$ complex, the imidazole ligand performs the function of a tag molecule and the dissociation from the complex, releasing free $[FePPIX]^+$, provides a fragmentation channel with relatively low threshold energy. IR multiple photon dissociation (IRMPD) spectroscopy has provided valuable information about structural and electronic features of a variety of gaseous charged species including nitrosyl iron−porphyrin complexes,[30−32] complexes of inorganic anions with π-acidic molecules,[33−37] and transition metal complexes of physiological or pharmacological relevance,[38−40] to name a few examples from the authors' work. Here, the target of the present contribution aims at identifying the presence of conformers in the sampled $[FePPIX(Im)]^+$ ion population.

2. EXPERIMENTAL METHODS

2.1. Materials. Hemin chloride ($Fe^{III}(PPIX)Cl$), methanol, dichloromethane, acetonitrile, ammonia, and imidazole were supplied by a commercial source (Sigma-Aldrich, Milan, Italy) and used without further purification. The $[FePPIX(Im)]^+$ complex was prepared by mixing in 1:1 solute molar ratio stock solutions of hemin chloride and imidazole 10^{-3} M in methanol. Solvent (either methanol or 1:1 dichloromethane/acetonitrile) was added to a final 10^{-5} M concentration, and NH_3 (ca. 5×10^{-6} M) was added to ensure a basic pH.

2.2. IRMPD Experiments. Two IR radiation sources, the free electron laser (FEL) at the Centre Laser Infrarouge d'Orsay (CLIO) facility and an optical parametric oscillator/amplifier (OPO/OPA) laser system at the Università di Roma "La Sapienza", were used to perform IRMPD experiments in the 900−1900 and 3000−3600 cm^{-1} spectral ranges, respectively.

The spectrum in the 900−1900 cm^{-1} range was recorded using a 7 T hybrid FT-ICR mass spectrometer (APEX-Qe Bruker) coupled to the CLIO FEL beamline. The experimental setup has been previously described in detail.[41] $[FePPIX(Im)]^+$ ions formed in solution were delivered in the gas-phase by an ESI source. Ions were accumulated and allowed to collide with argon in a quadrupole−hexapole interface and then pulse-extracted toward the FT-ICR cell. Here, mass-selected ions were stored and irradiated for 500 to 800 ms with IR-FEL light in the range of interest. For the present study, the electron energy was set to 43.5 MeV. When the IR light is in resonance with an active vibrational mode of the sampled ion, multiple events of photon absorption and intramolecular vibrational energy redistribution ultimately activate the fragmentation of the $[FePPIX(Im)]^+$ complex at m/z 684, yielding $[FePPIX]^+$ at m/z 616, as the unique dissociation product.

A LaserVision OPO/OPA laser coupled to a Paul ion trap mass spectrometer (Esquire 6000+, Bruker Inc.) was employed to explore the 3000−3600 cm^{-1} spectral range. As in the previously described experiment, the solution of the complex was directly infused with a syringe pump in the ESI source operated with conventional conditions. Two solvents were used (typically methanol and in a few experiments 1:1 dichloromethane/acetonitrile) in combination with different drying gas temperatures, at either the default value of 393 or 653 K. The OPO/OPA laser tunability within 2800−4000 cm^{-1} is bestowed by angle fine-adjusting of OPO and OPA crystals simultaneously. The typical output energy from the OPO/OPA laser was 20−21 mJ/pulse in the investigated spectral range. In the trap, ions were accumulated for 3 ms prior to IR irradiation. Multistage mass spectrometry was performed using the standard Bruker Esquire Control (v5.2) software. A typical irradiation time of 1 s was set by an electromechanical shutter synchronized with the mass spectrometer.

At each spectral frequency, four mass spectra were recorded and averaged. An IRMPD spectrum is obtained[42] by recording the photofragmentation yield R ($R = -\ln[I_{parent}/(I_{parent} + \Sigma I_{fragment})]$, where I_{parent} and $I_{fragment}$ are the integrated abundancies of the precursor and of the fragment ions,

DOI: 10.1021/jp5113476
J. Phys. Chem. B 2015, 119, 1919−1929

respectively) as a function of the wavenumber of the IR radiation,

2.3. Computational Details. To provide a comprehensive conformational survey and inspect candidate structures for the sampled ion population, DFT calculations have been performed using the Gaussian 09 program package.[43] The reported geometries have been optimized in the ground quartet state (doublet and sextet have been tested in few exemplary cases) at the UB3LYP/6-31G* level of theory, without any symmetry constraint. DFT offers an appropriate description of transition metal systems, including the first raw transition metal complexes, such as iron porphyrin complexes.[10,11,44,45] Because the choice of the functional is critical for the prediction of the spin ground state,[13,46−48] also BP86 and M06L have been tested for one exemplary $[FePPIX(Im)]^+$ conformer. However, B3LYP is known to offer the most cost-effective choice for the prediction of the molecular vibrational properties and IR spectra,[29,49] the focus of the present study. In the conformational survey, six of the nine starting geometries of the iron porphyrin complex, to be subsequently associated with the axial imidazole ligand, were extracted from a conformational analysis of $[FePPIX]^+$ by Siu et al.[22] In that seminal work, DFT-based molecular dynamics simulations were performed, and six representative conformers were selected and optimized using Vienna Ab initio Simulation Package (VASP) and Gaussian 03 programs. A good agreement was found between the calculated Boltzmann distribution of conformers at the temperature of the experiment and the results of the ion mobility measurements.

In the present work, one more conformer of $[FePPIX]^+$ has been taken into account. To these selected conformers an axial imidazole ligand was added (in two conformers imidazole is bound at either one of the nonequivalent axial positions) to build nine $[FePPIX(Im)]^+$ complexes, which have been submitted to energy minimization at the UB3LYP/6-31G* level of theory. Frequency analysis was performed at the same level of theory. Single point energy calculations were carried out at the UB3LYP/6-311+G** level for all nine complexes on the geometries optimized at the smaller UB3LYP/6-31G* level. Unless stated otherwise, the quartet spin state is considered throughout.

For direct comparison with the measured IRMPD spectra, the frequency-scaled calculated vibrational line spectra were convoluted using a Lorentzian line shape function with a full width at half-maximum (fwhm) value of 12 and 5 cm^{-1} in the 900−1900 and 3000−3600 cm^{-1} ranges, respectively. A frequency scaling factor of 0.973 was chosen in the 900−1900 cm^{-1} range,[32] while a value of 0.967 was adopted in the 3000−3600 cm^{-1} range. Additional gas-phase thermodynamic data were gained at 373 and 563 K.

3. RESULTS AND DISCUSSION

3.1. Experimental IR Spectrum of the Naked Iron(III)−Heme Imidazole Complex. The structural investigation of the $[FePPIX(Im)]^+$ complex, released from solution into the gas-phase by electrospray ionization, has relied on vibrational spectroscopy. To this end, the gaseous ions have been sampled by IRMPD spectroscopy. Though not based on a direct, one photon process, IRMPD spectroscopy typically yields a faithful description of the active vibrational modes, at least in terms of IR frequency. The ESI mass spectrum is shown in Figure S1 in the Supporting Information. As illustrated in Figure S2 (Supporting Information), the ion at m/z 684, corresponding to $[FePPIX(Im)]^+$, releases neutral imidazole forming a fragment ion at m/z 616 when irradiated with IR photons in resonance with an active vibrational mode. The loss of the axial ligand is clearly the least demanding dissociation pathway, largely favored with respect to fragmentations involving the porphyrin ligand.[12,50] Figure 2 shows the complete IRMPD

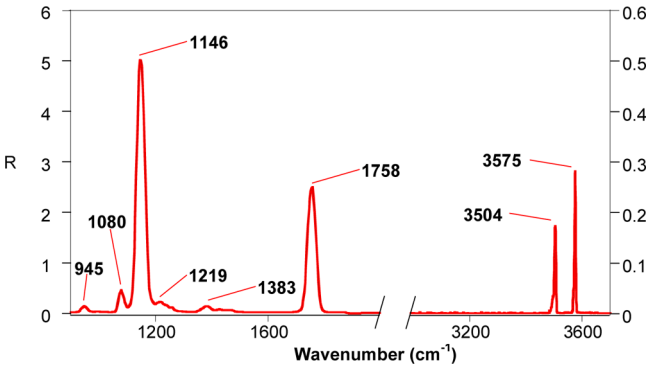

Figure 2. IRMPD spectrum of the naked $[FePPIX(Im)]^+$ complex.

spectrum of the $[FePPIX(Im)]^+$ complex, spanning both the "fingerprint" and the NH/OH stretching regions at 900−1900 and 3000−3600 cm^{-1}, respectively. Several signatures are observed. The low frequency region is dominated by a band at 1758 cm^{-1}, likely associated with the C═O stretching mode, and by a second one at 1146 cm^{-1}. Less pronounced bands are also observed at 945, 1080, 1219, and 1383 cm^{-1}.

In the 3000−3700 cm^{-1} range, two prominent bands appear at 3504 and 3575 cm^{-1} that can reasonably be assigned to the N−H stretching of the imidazole ligand and to the O−H stretch of the PrA groups on the porphyrin macrocycle, respectively.[51,52] In the attempt to reveal additional vibrational features in this region, an IRMPD spectrum has been recorded using an auxiliary CO_2 laser.[53] However, even this means of activating the IR induced fragmentation process failed to reveal any significant band in the carefully inspected 2900−3300 cm^{-1} range as shown in the IRMPD spectrum reported in Figure S3 (Supporting Information). The information attached to IRMPD spectra may be fruitfully taken advantage of when the experimental spectra are evaluated against the IR spectra expected for the plausible isomers that may comprise the sampled ion population. A computational survey of these isomers is described in the following paragraph.

3.2. Calculated Structures and Energetics for the Iron(III)−Heme Imidazole Complex. The $[FePPIX]^+$ ion is characterized by the presence of substituents on the periphery of the porphyrin ligand which are potentially very flexible. This flexibility allows the ion to sample a variety of different conformations and to establish different noncovalent interactions within the host heme protein depending on the mutual influence of heme conformation and arrangement of amino acid residues lining the cavity. The result is a fine-tuning of the heme enzymatic activity. In this study, the naked heme, $[FePPIX]^+$, engages an imidazole axial ligand and the combination of the ligand binding and orientation within the complex with several rotational isomers due to the presence of the porphyrin substituents generates a rich family of possible conformers. The main geometrical features of nine representative ones is detailed below. The relevant structural themes are illustrated with reference to Figure 3.

A characteristic structural motif concerns the PrA groups that may be more or less involved in intramolecular hydrogen

DOI: 10.1021/jp5113476
J. Phys. Chem. B 2015, 119, 1919−1929

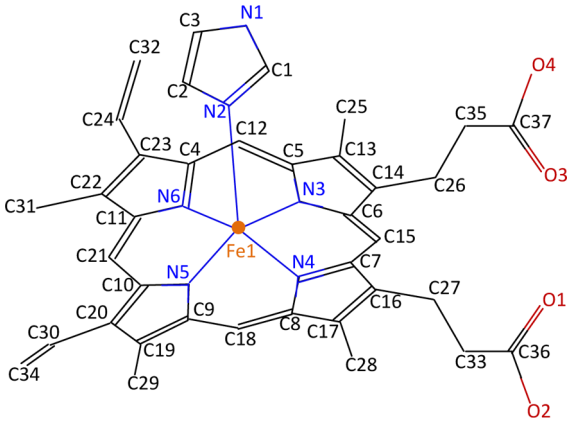

Figure 3. Schematic drawing of the heme−imidazole complex with assigned atom identity and numbering. Hydrogen atoms are not shown.

bonding. All conformers, whose geometries were optimized at the UB3LYP/6-31G* level, correspond to an energy minimum, as proven by frequency analysis. Their structures are depicted in Figure 4 in a compact way, whereas enlarged pictures are available in Figure S4 (Supporting Information).

Conformers **HemIm-1**, **HemIm-2**, and **HemIm-3** present PrA side chains that are free from H-bond interactions. They either stretch out on the porphyrin plane or bend in an approximately perpendicular direction to it. **HemIm-3** is similar to the heme conformation observed in a crystal structure (see Figure 1b). In contrast, in **HemIm-4**, **HemIm-5** and **HemIm-6** the two PrA groups are connected by either one or two (**HemIm-6**) hydrogen bonds. These geometries reproduce the structures of the six $[FePPIX]^+$ conformers calculated by Siu and co-workers,[22] only differing for the additional imidazole ligand. In conformer **HemIm-7**, the two PrA groups point in opposite direction with reference to the porphyrin plane, conforming to an arrangement already reported by Fornarini et al.[54] The two PrA groups present an orientation similar to that in **HemIm-2**, though in an inverted up/down arrangement relative to the porphyrin plane and the imidazole axial position. The structure of **HemIm-8** is related to the one of **HemIm-5**, where the innermost PrA group appearing in Figure 4 is removed from the "up" disposition relative to the porphyrin plane and the imidazole ligand and oriented downward. The last structure, namely, **HemIm-9**, presents an arrangement of the PrA groups quite similar to the one in conformer **HemIm-6**, with a double H-bond interaction. However, in **HemIm-6** the imidazole ligand and the PrA groups are on the same side relative to the porphyrin plane, while in **HemIm-9** the PrA groups stretch out on the other side of the plane with respect to imidazole.

Interestingly, the carbonyl oxygen of a PrA substituent may not only be involved in H-bonding with a hydroxyl hydrogen of the neighboring PrA group but also be involved in CH···O═C close contacts with hydrogen atoms belonging to imidazole, which are quite common in protein structures and are considered genuine though weak.[55,56] These H atoms are positively polarized due to the metal−ligand bonding, and their interaction with the carbonyl groups is highlighted by dotted lines in Figure 4. Imidazole-H···O═C distances of 2.30−2.47 Å are rather long, though, when compared to a typical OH···O═C distance of 1.76 Å as found, for example, in **HemIm-4**. This CH···O═C structural motif may be recognized in structures **HemIm5**, **HemIm-6**, **HemIm-7**, and **HemIm-8** (see Figure 4). In the case of **HemIm-5**, the N−H bond pointing upward is close enough to establish also a weak hydrogen bond with the

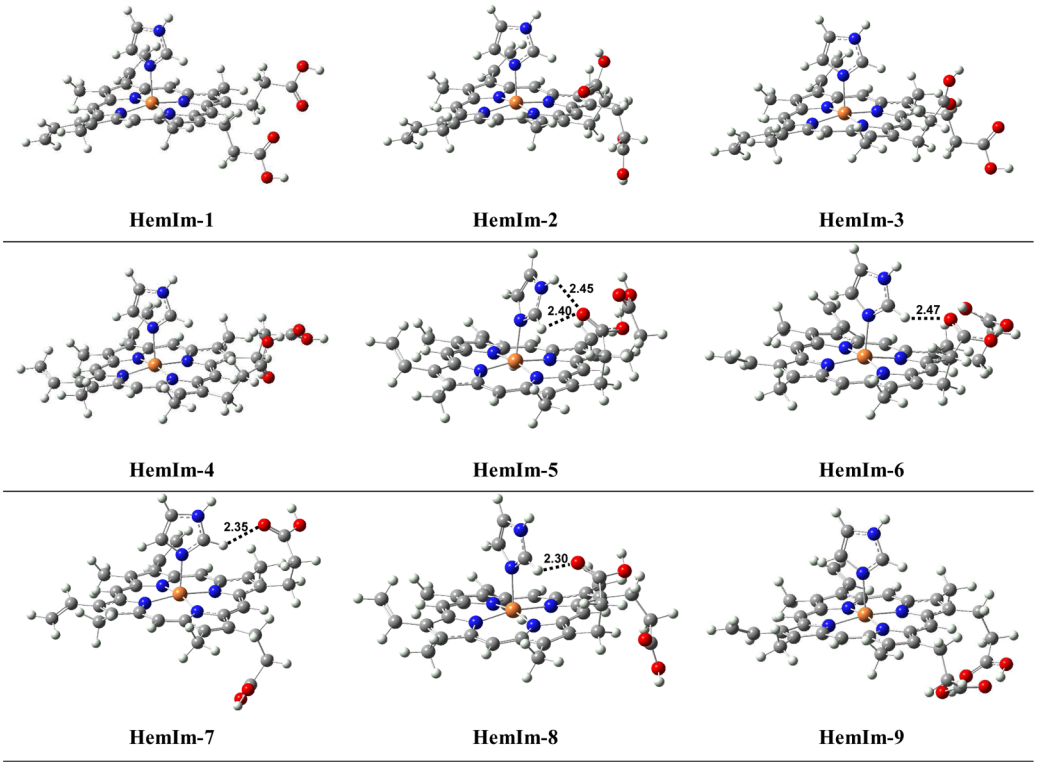

Figure 4. Most stable optimized geometries of $[FePPIX(Im)]^+$ isomers calculated at the UB3LYP/6-31G* level of theory. Hydrogen bonds involving the imidazole ligand are shown as dotted lines (length in Å).

DOI: 10.1021/jp5113476
J. Phys. Chem. B 2015, 119, 1919−1929

PrA C═O group characterized by a NH···O═C distance of 2.45 Å.

Geometrical parameters are listed in Table 1, reporting also the experimental values obtained from a solid state X-ray diffraction experiment on CYP51, a prototypical heme enzyme holding an imidazole ligand from 1-[3-(4-chloro-3,5-dimethylphenoxy)benzyl]-1*H*-imidazole, axially coordinated to the heme prosthetic group.[57] Nonetheless, differences should be expected, primarily because the X-ray data were extracted for the solid state, whereas the theoretical data refer to isolated complexes, and also because the X-ray resolution (2.80 Å) includes approximately 5% experimental error.[58]

Table 1. Geometrical Parameters for [FePPIX(Im)]$^+$ Conformers Compared with the Experimental Parameters Extracted from the Crystal Structure of CYP51 (PDB: 4H6O)[a]

	distance	dihedral	angle
name	Fe1−N2	N4−Fe1−N2−C1	N4−Fe1−N2
HemIm-1	2.14	33.29	94.59
HemIm-2	2.14	46.40	94.55
HemIm-3	2.14	49.57	95.37
HemIm-4	2.14	40.32	95.83
HemIm-5	2.13	1.39	93.88
HemIm-6	2.14	27.81	93.95
HemIm-7	2.14	74.83	96.96
HemIm-8	2.13	7.45	95.09
HemIm-9	2.14	45.08	96.08
Exp	2.04	43.72	87.00

[a]Distances are in Å and angles and dihedrals in degrees.

The Fe1−N2 bond in the nine conformers has approximately constant length as obtained by ab initio calculations at UB3LYP/6-31G* level, somewhat larger than the experimental value (2.04 Å). A slight decrease appears in **HemIm-5** and **HemIm-8**, possibly as a consequence of the interaction between imidazole and a PrA group. In all of the computed structures, the Fe1−N2 bond is orthogonal to the heme plane, as in the crystal structure (see Figure 1). The theoretical bond angle N4−Fe1−N2 is also reported in Table 1 appearing slightly larger than the experimental value, as if the imidazole ligand were driven away by the PrA groups. The lowest values are observed in the structure of **HemIm-5** and **HemIm-6** (93.88° and 93.95°, respectively), where imidazole hydrogen atoms interact by H-bonding with a PrA group. A trend in the computed N4−Fe1−N2−C1dihedral angles may also be recognized. Starting from the experimental angle of 43.72°, where the ligand plane approximately bisects the N4−Fe1−N3 angle, some deviations have been observed in the computed geometries. In the **HemIm-5** and **HemIm-8** complexes, the dihedral angle is small and drops almost to zero, while in **HemIm-7** the angle is much larger (74.43°) than the experimental one. These unusual values can be traced to the different position of the carbonyl oxygen atoms engaged in hydrogen bonding with imidazole and to the rotation of the ligand plane to allow a proper interaction. In the absence of such interactions, for example, in **HemIm-9**, the value of the dihedral angle (45.08°) is very close to the experimental one, and the imidazole plane effectively bisects the N4−Fe1−N3 angle. An angle of 45° is consistent with the notion that the imidazole ligand may withstand the least steric hindrance with the pyrrole nitrogens when it is not aligned along a Fe−N(pyrrole) bond.[13,59]

In the full heme complex, it emerges clearly from these computational results that the presence and orientation of the porphyrin substituents have an influence on the arrangement of the axial ligand and, possibly, may affect the robustness of the formed complex.

Relative energies of the selected conformers are obtained by single point energy calculations carried out at the UB3LYP level using the 6-311+G** basis set and are reported in Table 2. Relative enthalpy and free energy values are reported at two different temperatures, 373 and 563 K, related to the adopted experimental conditions. The trend in the relative electronic energy and enthalpy values confirms the role of intramolecular hydrogen bonding in determining the relative stability of the conformers. The two H bonds linking the PrA groups stabilize **HemIm-6** and, to a lesser extent, **HemIm-9**. The latter isomer is close in energy to **HemIm-5**, characterized by a single H-bond between the PrAs and by the presence of two weak imidazole-NH···O═C and imidazole-CH···O═C bonds. Species with free PrAs, namely, **HemIm-1**, **HemIm-2**, **HemIm-3**, and **HemIm-7**, are higher in energy, while a beneficial effect by an imidazole-CH···O═C interaction is probably operating in **HemIm-8**.

Considering the relative free energies, the overall span between the various isomers is remarkably reduced, and species that are highest in energy such as **HemIm-1**, **HemIm-2**, and **HemIm-3** are now among the most likely candidates. This finding is a result of the higher entropy imparted by the free PrAs. In contrast, entropic factors affect adversely the

Table 2. Relative Electronic Energy and Zero Point Energy (ZPE) for Selected [FePPIX(Im)]$^+$ Conformers[a]

species	$\Delta E^{b,c}$	ZPE^{c,d}	$\Delta H_{373\ K}{}^{c,d}$	$\Delta G_{373\ K}{}^{c,d}$	$\Delta H_{563\ K}{}^{c,d}$	$\Delta G_{563\ K}{}^{c,d}$
HemIm-1	8.7	421.3	8.3	0.6	8.6	0.0
HemIm-2	8.2	421.8	7.9	2.1	8.2	2.3
HemIm-3	7.6	421.6	7.3	0.4	7.7	0.1
HemIm-4	4.6	422.6	4.7	2.5	4.8	4.7
HemIm-5	2.2	422.9	2.3	1.9	2.5	5.0
HemIm-6	0.0	423.5	0.0	0.0	0.0	3.3
HemIm-7	7.4	422.3	7.4	3.3	7.7	4.5
HemIm-8	4.7	422.2	4.6	0.5	4.9	1.7
HemIm-9	2.4	423.4	2.6	3.4	2.6	7.2

[a]Relative enthalpy and Gibbs free energy are reported at two different temperatures. [b]Relative electronic energies obtained by single point calculations performed at the UB3LYP/6-311+G** level of theory. [c]In kcal mol^{-1}. [d]Zero point energy (ZPE) and thermal enthalpy and free energy contributions have been obtained at the UB3LYP/6-31G* level of theory.

DOI: 10.1021/jp5113476
J. Phys. Chem. B 2015, 119, 1919−1929

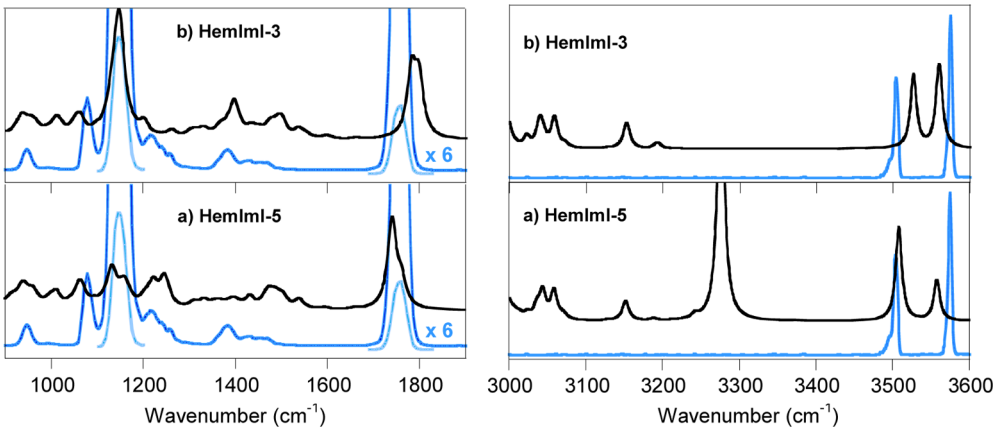

Figure 5. Theoretical IR spectra (black) of (a) **HemIm-5** and (b) **HemIm-3**, obtained at the UB3LYP/6-31G* level of theory, plotted together with the IRMPD spectrum (blue) of $[FePPIX(Im)]^+$. The laser beam was attenuated (by a factor of 6) in the light blue profile.

conformers that present intramolecular hydrogen bonding and more folded structures such as **HemIm-6** and **HemIm-9** but also, to a lesser extent, **HemIm-5**. The entropic contribution to the relative free energy values becomes obviously more pronounced as the temperature is increased.

Because multiple spin states may account for five-coordinate $[FePPIX(Im)]^+$ complexes, the **HemIm-8** conformer has been selected for a comparative survey of the potentially accessible sextet and doublet states (S = 5/2, 1/2, respectively) besides the routinely accepted quartet (S = 3/2). Calculations based on **HemIm-8** confirm the quartet spin state to be the ground state both for the bound heme, $[FePPIX(Im)]^+$, and for the free ion, $[FePPIX]^+$. The doublet and the sextet spin states of $[FePPIX(Im)]^+$ are higher in energy by 20.0 and 15.2 kcal mol^{-1}, respectively, in general agreement with previous reports on closely related systems.[12,60] In contrast, five coordinate complexes with a negatively charged ligand (e.g., thiolate as in P450 model complexes) are known to rather prefer the higher spin state.[10,14,45] As a further control, calculations have been run on **HemIm-5** using two different functionals, BP86 and M06L. The quartet state is consistently found to be the ground state, although the ordering of the higher lying doublet and sextet is different.

In the ground quartet state, also the Fe-Im binding energy for the $[FePPIX(Im)]^+$ complex has been evaluated, subtracting the enthalpy of the complex from the sum of the enthalpies of the fragments imidazole and $[FePPIX]^+$, at 373 K. Calculations at the UB3LYP/6-311G**//UB3LYP/6-31G* level using **HemIm-6** as the structure of the bound species and the corresponding geometry also for the free heme ion yield a value of 27.4 kcal mol^{-1}, comparable with the imidazole binding energy of other transition metal porphyrin complexes in the gas-phase.[61]

3.3. Vibrational Features of Sampled $[FePPIX(Im)]^+$ Conformers. The main purpose of this work is to gain structural insight about the sampled $[FePPIX(Im)]^+$ ion. To this end, the IRMPD spectra are inspected against the calculated IR spectra of the various conformers. The complete array of vibrational spectra is provided in Figures 5 and S5 (Supporting Information), showing the calculated IR spectra for **HemIm-1** to **HemIm-9** species (black profiles) plotted together with the experimental IRMPD spectrum (blue profiles).

Few points that emerge from the comparison between calculated IR spectra and the experimental IRMPD spectrum may be emphasized. The IR spectrum of the most stable structure, namely, **HemIm-6**, does not reproduce the experimental data. The pronounced band at 1146 cm^{-1} may rather be ascribed to an unfolded conformer such as **HemIm-1** and **HemIm-2** (Figure S5, Supporting Information) or **HemIm-3** (Figure 5). However, there is not a single isomer that may account for the sampled $[FePPIX(Im)]^+$ ion in the two spectral regions explored, though all experimental features are backed in the calculated IR spectra of the various conformers. This view is also suggested by the relatively large bandwidth of the most prominent bands. For example, the band at 1758 cm^{-1} associated with the C═O stretching of the PrAs may include the contribution of both H-bonded and unfolded isomers. As exemplary IR spectra, Figure 5 displays the spectra calculated for **HemIm-3** and **HemIm-5**, representative conformers of unfolded (**HemIm-3**: no hydrogen bonds) and folded (**HemIm-5**: one hydrogen bond) species. The set of IR spectra calculated for the various conformers is completed in Figure S5 (Supporting Information). **HemIm-3** and **HemIm-5** are used as reference also in Table 3, listing experimental IRMPD features and IR modes calculated for the two selected conformers.

The analysis of the tabulated data confirms the qualitative agreement between experimental and calculated IR modes in the spectra reported in Figure 5. In particular, one may note that the two small bands at 945 and 1080 cm^{-1} result from at least four different modes. The first two, at 959 and 952 cm^{-1}, can be assigned to vinyl CH_2 rocking and porphyrin ring breathing, strongly coupled modes for **HemIm-5** and **HemIm-3**, respectively. The other two, at 1061 cm^{-1} in both conformers, involve the in plane deformation of the imidazole ring.[62] The sharp profile of the experimental band at 1080 cm^{-1} may be ascribed to the rigid, planar structure of the heteroaromatic ring.[63] Bands associated with C−O−H bending within the PrA groups are computed to appear in the 1137−1153 cm^{-1} range in the **HemIm-3** spectrum, while the broad feature observed experimentally around 1219−1230 cm^{-1} may be associated with modes computed at 1223 and 1247 cm^{-1} in the **HemIm-5** conformer.

The strong absorption at 1758 cm^{-1} is accounted for by the C═O stretching mode calculated at 1742−1798 cm^{-1} since its shape and width suggest the presence of two or more overlapping bands, probably due to the presence of folded PrA groups (see Figure S5 (Supporting Information) for calculated spectra of other isomers). If only **HemIm-3** with

DOI: 10.1021/jp5113476
J. Phys. Chem. B 2015, 119, 1919−1929

Table 3. Experimental IRMPD Bands and Calculated (at the UB3LYP/6-31G* Level) Vibrational Frequencies for [FePPIX(Im)]$^+$ in the 900−1900 and 3000−3600 cm^{-1} Range

Exp IRMPD[a]	calcd IR[b,c] in [HemIm-5]$^+$	calcd mode[b,c] in [HemIm-3]$^+$	mode description
945	912 (24)	952 (44)	porphyrin ring breathing
	935 (24), 936 (22)	963 (36), 936 (25), 933 (28)	CH_2 wagging
	943 (36), 959 (41)	1008 (26), 1011 (28)	vinyl CH_2 rocking
	964 (23), 1011 (22), 1012 (34)	1096 (21)	CH in plane bending
1080	1061 (66)	1130 (37), 1061 (70)	imidazole ring deformation
	1154 (37)	1363 (21)	CH in plane bending
1146	1128 (31), 1134 (121)	1127 (27)	Porphyrin ring breathing
	1068 (53), 1160 (32)	1199 (59)	CH_2 twisting
	1164 (40)	1144 (79), 1149 (194), 1153 (42), 1137 (107)	C−O−H in plane bending
1219	1203 (34), 1216 (26)		CH out of plane bending
	1223 (79), 1247 (92)		C−O−H in plane bending
1383	1398 (26)	/	C−O−H in plane bending
	1431 (21), 1505 (41)	1501 (50)	imidazole ring deformation
	1475 (21), 1488 (20)	1494 (24)	CH_2 scissoring
	/	1329 (72), 1396 (82), 1398 (56)	CH_2 wagging
1758	1742 (383)	1781 (280)	C═O asymm stretching
	1762 (105)	1798 (244)	C═O symm stretching
	3056 (21), 3059 (21)	3058 (22), 3060 (20)	vinyl CH stretching
	3276 (438)	/	OH stretching
3504	3508 (137)	3525 (111)	imidazole N−H stretching
3575	3558 (59)	3560 (36), 3561 (119)	O−H stretching

[a]Experimental frequency (cm^{-1}). [b]Calculated IR frequencies (cm^{-1}) and intensities (km mol^{-1}, in parentheses). IR modes involving the same vibration type are grouped together. [c]Modes with computed intensities smaller than 20 km mol^{-1} are omitted for the sake of clarity.

unfolded PrAs were present, the C═O stretching mode would appear at higher frequency (1781−1798 cm^{-1}). However, the calculated spectrum of the **HemIm-3** structure is consistent with the major features in the experimental spectrum, indicating that this one or similar structures are likely dominant in the experimental ion population. The **HemIm-5** structure is characterized by a carbonyl oxygen (O1) of one PrA group that is involved in hydrogen-bonding with imidazole in a 2-fold interaction, while the hydroxyl hydrogen of the same group is hydrogen bonded to O3. These two structural motifs are reflected in the calculated spectra, where the C═O stretch is substantially red-shifted from that of the **HemIm-3** conformer and the in-plane hydroxyl bend is considerably weaker. Red shift effects in the C═O stretching mode of carboxylic acid functionalities involved in hydrogen bonding are well documented in IRMPD spectroscopy.[64] Finally, a weak and unstructured signature at 1383 cm^{-1} can be associated with several coupled modes with a major contribution from the wagging motion of the CH_2 group of the **HemIm-3** conformer.

In the 3000−3600 cm^{-1} region displayed in the right portion of Figure 5, the computed IR spectra confirm the assignment of the two distinct bands at 3504 and 3575 cm^{-1} to N−H stretching of the imidazole ligand and to O−H stretch, respectively. The experimental features are more widely separated (by 71 cm^{-1}) than the computed transitions (50 and 36 cm^{-1} in the IR spectra of **HemIm-5** and **Hem-Im-3**, respectively). No appreciable IRMPD feature appears at lower frequency, in spite of careful search. The C−H stretching modes are known to be weak and are not expected to yield signals of any significant intensity in a spectral region that starts to be adversely affected by the decreasing power of a laser. In contrast, calculations predict remarkable intensity for O−H stretching modes involved in hydrogen bonding as in the spectrum of isomer **HemIm-5** reported in Figure 5 (at 3276 cm^{-1}) and in the IR spectra of folded conformers **HemIm-4**, **HemIm-6**, and **HemIm-9** displayed in Figure S5 (in the 3120−3230 cm^{-1} range; Supporting Information). The fact that no such feature appears in the interested spectral range cannot, however, be considered as negative evidence for the presence of H-bonded conformers. It is often recognized that IR modes involved in a hydrogen bond network fail to fulfill the transition position and intensity predicted by harmonic calculations when they are sampled by IRMPD spectroscopy. Several effects may cause unexpectedly weak or absent features including the nonlinear behavior attached to IRMPD spectroscopy, the strong anharmonicity expected in particular when the proton binding sites are similar in proton affinity, and the breaking of the hydrogen bond along the stepwise multiple photon absorption process.[65−67]

In conclusion, the lack of any significant signal in the range where strongly H-bonded hydroxyl groups are expected to absorb does not exclude the presence of folded conformers. However, the experimental IRMPD spectrum displayed in Figure 5 shows a remarkable intensity for the stretching mode of free O−H at 3575 cm^{-1} with respect to the imidazole N−H stretching band. These relative intensities are better reproduced in the calculated IR spectra of unfolded conformers such as **HemIm-3**, rather than in folded ones such as **HemIm-5** where the O−H stretch of the hydroxyl group engaged in H-bonding is red-shifted and likely to exhibit weakened IRMPD activity. Overall, the IRMPD spectrum of the sampled [FePPIX(Im)]$^+$ ion is consistent with a dominant contribution of unfolded conformers.

3.4. Evidence for the Presence of Multiple [FePPIX(Im)]$^+$ Conformers. Evidence for the existence of multiple conformers in the sampled [FePPIX(Im)]$^+$ ion population is obtained when changing the experimental conditions, such as ESI solvent and drying gas temperature. The analysis is based on the distinct signatures in the NH/OH stretching region. Table 4 summarizes the details of experiments performed varying drying gas temperature (II) and solvent (III and IV). In column five, the signal integral for the two bands at 3504 and 3575 cm^{-1} is reported. The absolute values bear no direct information because the IRMPD yield for the same mode recorded in different runs may reflect instrumental factors such as the spacial overlap of the IR beam with the ion cloud, which are not easily and routinely controlled. Relative absorption intensities, however, are meaningful, and measurable differences are recorded for the two bands which suggest a varying

DOI: 10.1021/jp5113476
J. Phys. Chem. B 2015, 119, 1919−1929

Table 4. IRMPD Experiments on the Two Distinct Vibrational Signatures of [FePPIX(Im)]$^+$ in the NH/OH Stretching Range

exp	T^a	solvent^b	signature	signal integral	NH/OH ratio^c
I	563	CH_3OH	NH	1.43	0.83
			OH	1.72	
II	373	CH_3OH	NH	2.97	1.56
			OH	1.90	
III	563	CH_2Cl_2/CH_3CN (1:1)	NH	2.63	NH
			OH	2.10	
IV	373	CH_2Cl_2/CH_3CN (1:1)	NH	2.72	1.56
			OH	1.74	

^{a}Drying gas temperature (K). ^{b}ESI solvent. ^{c}Estimated error ±10%.

conformer distribution depending on the sampling conditions of [FePPIX(Im)]$^+$ ions.

One may expect that an increasing presence of folded conformers should bring about a decrease in the relative intensity of the free O−H band so that the ratio between the integrated signals for N−H and free O−H stretching modes will increase. In fact, it is already clear from the computed IR spectra in Figure 5 that in the presence of just one O−H group involved in H-bonding, as in isomer **HemIm-5**, the intensity of the stretching mode of free O−H is noticeably weaker relative to the N−H stretching band, when compared with that of an unfolded conformer such as **HemIm-3**. Therefore, the ratio between the integrated signals for N−H and free O−H stretching modes may be taken as a measure of the relative proportion of folded and unfolded conformers. The values reported in Table 4 suggest that increasing the drying gas temperature favors the presence of unfolded conformers. For example, using methanol as solvent the NH/OH ratio varies from 1.56 at 373 K to 0.83 at 563 K. This finding is in agreement with the thermodynamic data reported in Table 2 showing that at 563 K unfolded structures such as **HemIm-1** and **HemIm-3** become the favored ones in terms of free energy. The temperature effect is observed using either methanol as solvent or a 1:1 mixture of CH_2Cl_2 and CH_3CN (see Exp III and Exp IV). In both instances, the higher drying gas temperature appears to have an influence on the internal energy content of the sampled ion releasing a higher fraction of unfolded species. In contrast, using an aprotic solvent mixture, CH_2Cl_2/CH_3CN, in the place of methanol rather favors the folded conformers. Once again, this point is evinced from a change in the ratio between the integrated signals for N−H and free O−H stretches which varies from 0.83 using methanol to 1.25 using CH_2Cl_2/CH_3CN, at the temperature of 563 K. It is plausible that the aprotic solvent, unable to ensure hydrogen-bond interactions with the PrA groups, may favor the intramolecular interaction in the folded conformation which is then released in higher proportion in the ESI process.

The described phenomena in relative band intensity reflect a consistently reproduced behavior in experiments independently run in different months. Figure 6 shows a plot of the IR range including the N−H and free O−H stretching bands at 3504 and 3575 cm^{-1} with the red and blue profiles depicting the spectra recorded for Exp I and Exp II, respectively. One may note that, as already stated, the O−H stretch band is weaker in intensity in Exp II and also that a shoulder on the low frequency side of the N−H stretching band at 3504 cm^{-1} becomes more pronounced. It is tempting to assign this

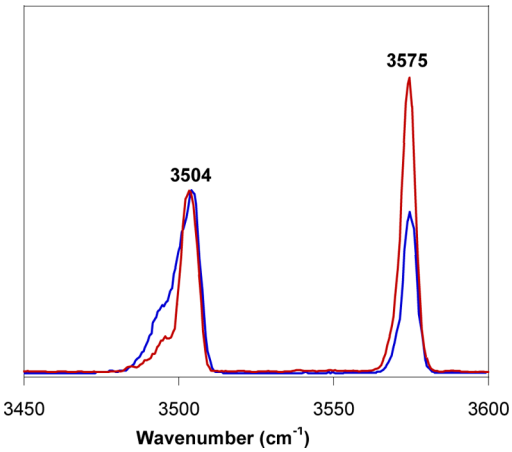

Figure 6. IRMPD spectra of the [FePPIX(Im)]$^+$ complex in the 3450−3600 cm^{-1} range. Red and blue profiles correspond to Exp I and Exp II, respectively. In order to make graphical analysis clearer, the N−H absorbance at 3504 cm^{-1} for the two experiments has been normalized to the same maximum value.

shoulder as a feature of **HemIm-5**, characterized by the more widely parted N−H and free O−H stretching bands, whose relative abundance increases at the lower temperature of Exp II, in agreement with the partly folded character of this conformer. In the framework of the present results and their interpretation, it would be highly interesting to further change the drying gas temperature to lower values to possibly observe increasing prevalence of folded conformations. Unfortunately, any further decrease was not permitted in our instrument due to ion signal loss.

Ion-mobility experiments conducted in He, at 1 Torr, as buffer gas at 298 K have shown that the free [FePPIX]$^+$ complex presents internal hydrogen bonding between the two propionic acid substituents.[22] In the present study, the conformer distribution rather favors the unfolded conformers in the case of the [FePPIX(Im)]$^+$ complex sampled under lower pressure conditions and relatively high ESI operative temperatures.

4. CONCLUSIONS

An evaluation of the IRMPD spectrum of [FePPIX(Im)]$^+$ ions has been performed, and a comparative analysis has been allowed by the thorough survey of calculated IR spectra of the candidate isomers. It is confirmed that IRMPD spectroscopy coupled to a computational survey of candidate structures is a valuable approach to gain insight into the presence of multiple conformers in an ion population sampled in the gas-phase. This contribution was aimed at elucidating the role played by intramolecular hydrogen-bonding in the conformational landscape of the five-coordinate heme complex with an imidazole ligand. To this end, geometries and IR spectra obtained for nine eligible candidates have been analyzed, allowing vibrational mode assignment for the IRMPD bands of the [FePPIX(Im)]$^+$ complex. The possible stable conformers of [FePPIX(Im)]$^+$ ion display relative energies in a range of about 9 kcal mol^{-1}. The geometries differ according to the orientation of the propionyl peripheral groups with respect to the porphyrin plane and to the imidazole ligand. Sensitive parameters are the N4−Fe1−N2−C1 dihedral angle and the N4−Fe1−N2 angle, which vary in concert with IR absorptions in the various structures. As seen from the calculated IR spectra, characteristic changes are

DOI: 10.1021/jp5113476
J. Phys. Chem. B 2015, 119, 1919−1929

brought about by the presence of hydrogen bonding interactions. For example, in the fingerprint region of the IR spectrum a distinct red-shift affects the C=O stretching frequencies of the **HemIm-5** conformer, with the PrA groups engaged in a hydrogen-bond interaction.

In the 3000−3600 cm^{-1} region, the IRMPD features suggest that at least one O−H group must be present that is not involved in hydrogen bonding. However, the frequency of this O−H stretching mode does not appreciably differentiate between selected conformers. Probably the most informative mode appears to be the imidazole N−H stretching, which is somewhat red-shifted when the hydrogen atom interacts with a carbonyl oxygen as verified in **HemIm-5**. Across a survey of IRMPD experiments run in the 3450−3600 cm^{-1} region, a variation is observed in the relative intensities of the two stretching modes, N−H and O−H, as the experimental conditions are modified. A higher temperature of the drying gas favors an increasing fraction of unfolded conformers as reflected by a smaller ratio between the band intensities of the NH/OH stretches, while folded conformers (e.g., **HemIm-5**) are preferred when the drying gas temperature is lower (373 K), or when the gaseous ions are generated from an aprotic solvent solution.

In summary, it is an interesting result that a good agreement between the measured infrared spectra and the computational spectral simulations has been found for such a relatively large system. Additionally, the gathered spectroscopic and computational evidence point to the existence of a mixed ion population comprising conformers whose PrA groups are involved in hydrogen-bonding interactions to a variable extent depending on environmental conditions.

■ ASSOCIATED CONTENT

Ⓢ Supporting Information

Full scan positive-ion ESI mass spectrum of a methanolic solution of imidazole and hemin chloride and IR induced mass spectrum of $[Fe^{III}PPIX(Im)]^+$ recorded at 3504 cm^{-1}; IRMPD spectrum of $[FePPIX(Im)]^+$ in the NH/OH stretch range, assisted by an auxiliary CO_2 laser; enlarged pictures of all the conformers computed for the $[FePPIX(Im)]^+$ complex at the UB3LYP/6-31G* level of theory and experimental IRMPD spectra of $[FePPIX(Im)]^+$ together with computed IR spectra of **HemImI-1**, **HemIm-2**, **HemIm-4**, **HemIm-6**, **HemIm-7**, **HemIm-8**, and **HemIm-9**, all calculated at the UB3LYP/6-31G* level in the wavenumber range of 900−1900 cm^{-1} and 3000−3600 cm^{-1}; and complete reference for Gaussian 09 and ref 55. This material is available free of charge via the Internet at http://pubs.acs.org.

■ AUTHOR INFORMATION

Corresponding Author

*E-mail: simonetta.fornarini@uniroma1.it.

Notes

The authors declare no competing financial interest.

■ ACKNOWLEDGMENTS

We are grateful to Philippe Maitre, Vincent Steinmetz, Debora Scuderi, Joel Lemaire, Jean-Michel Ortega, and to the technical team at CLIO. We thank K. W. Michael Siu for the information provided on computed $[FePPIX]^+$ geometries. This work was supported by the Università degli Studi di Roma La Sapienza (Prot. C26A13544B) and by the European Commission (CLIO project IC014-13). The assistance provided by Annito Di Marzio for experiments at the OPO/OPA laser is gratefully acknowledged.

■ REFERENCES

(1) Holm, R. H.; Kennepohl, P.; Solomon, E. I. Structural and Functional Aspects of Metal Sites in Biology. *Chem. Rev.* **1996**, *96*, 2239−2314.

(2) Loew, G. H.; Harris, D. L. Role of the Heme Active Site and Protein Environment in Structure, Spectra, and Function of the Cytochrome P450s. *Chem. Rev.* **2000**, *100*, 407−420.

(3) Sono, M.; Roach, M. P.; Coulter, E. D.; Dawson, J. H. Heme-Containing Oxygenases. *Chem. Rev.* **1996**, *96*, 2841−2888.

(4) Woggon, W. D. Metalloporphyrines as Active Site Analogues-Lessons from Enzymes and Enzyme Models. *Acc. Chem. Res.* **2005**, *38*, 127−136.

(5) Lombardi, A.; Nastri, F.; Pavone, V. Peptide-Based Heme-Protein Models. *Chem. Rev.* **2001**, *101*, 3165−3189.

(6) Cerda, J. F.; Malloy, M. C.; Werkheiser, B. O.; Stockhausen, A. T.; Gallagher, M. F.; Lawler, A. C. Evaluation of Heme Peripheral Group Interactions in Extremely Low-Dielectric Constant Media and Their Contributions to the Heme Reduction Potential. *Inorg. Chem.* **2014**, *53*, 182−188.

(7) Gilson, M. K.; Honig, B. H. The Dielectric Constant of a Folded Protein. *Biopolymers* **1986**, *25*, 2097−2119.

(8) Warshel, A.; Dryga, A. Simulating Electrostatic Energies in Proteins: Perspectives and Some Recent Studies of pkas, Redox, and Other Crucial Functional Properties. *Proteins* **2011**, *79*, 3469−3484.

(9) Galstyan, A. S.; Zaric, S. D.; Knapp, E. W. Computational Studies on Imidazole Heme Conformations. *J. Biol. Inorg. Chem.* **2005**, *10*, 343−354.

(10) Shaik, S.; Kumar, D.; de Visser, S. P.; Altun, A.; Thiel, W. Theoretical Perspective on the Structure and Mechanism of Cytochrome P450 Enzymes. *Chem. Rev.* **2005**, *105*, 2279−2328.

(11) Charkin, O. P.; Klimenko, N. M.; Charkin, D. O.; Chang, H. C.; Lin, S. H. Theoretical DFT Study of Fragmentation and Association of Heme and Hemin. *J. Phys. Chem. A* **2007**, *111*, 9207−9217.

(12) Charkin, O. P.; Klimenko, N. M.; Nguyen, P. T.; Charkin, D. O.; Mebel, A. M.; Lin, S. H.; Wang, Y. S.; Wei, S. C.; Chang, H. C. Fragmentation of Heme and Hemin$^+$ with Sequential Loss of Carboxymethyl Groups: A DFT and Mass Spectrometry Study. *Chem. Phys. Lett.* **2005**, *415*, 362−369.

(13) Smith, D. M.; Dupuis, M.; Vorpagel, E. R.; Straatsma, T. P. Characterization of Electronic Structure and Properties of a bis-(Histidine) Heme Model Complex. *J. Am. Chem. Soc.* **2003**, *125*, 2711−2717.

(14) Balding, P. R.; Porro, C. S.; McLean, K. J.; Sutcliffe, M. J.; Maréchal, J.-D.; Munro, A. W.; de Visser, S. P. How Do Azoles Inhibit Cytochrome P450 Enzymes? A Density Functional Study. *J. Phys. Chem. A* **2008**, *112*, 12911−12918.

(15) Chen, O. N.; Groh, S.; Liechty, A.; Ridge, D. P. Binding of Nitric Oxide to Iron(II) Porphyrins: Radiative Association, Blackbody Infrared Radiative Dissociation, and Gas-Phase Association Equilibrium. *J. Am. Chem. Soc.* **1999**, *121*, 11910−11911.

(16) Hayes, L. A.; Chappell, A. M.; Jellen, E. E.; Ryzhov, V. Binding of Metalloporphyrins to Model Nitrogen Bases: Collision-Induced Dissociation and Ion−Molecule Reaction Studies. *Int. J. Mass. Spectrom.* **2003**, *227*, 111−120.

(17) Angelelli, F.; Chiavarino, B.; Crestoni, M. E.; Fornarini, S. Binding of Gaseous Fe(III)-Heme Cation to Model Biological Molecules: Direct Association and Ligand Transfer Reactions. *J. Am. Soc. Mass Spectrom.* **2005**, *16*, 589−598.

(18) Crestoni, M. E.; Fornarini, S. Heme-Peptide/Protein Ions and Phosphorous Ligands: Search for Site-Specific Addition Reactions. *J. Biol. Inorg. Chem.* **2007**, *12*, 22−35.

(19) Chiavarino, B.; Crestoni, M. E.; Fornarini, S.; Rovira, C. Unravelling the Intrinsic Features of NO Binding to Iron(II)- and Iron(III)-Hemes. *Inorg. Chem.* **2008**, *47*, 7792−7801.

DOI: 10.1021/jp5113476
J. Phys. Chem. B 2015, 119, 1919−1929

(20) Pashynska, V. A.; Van den Heuvel, H.; Claeys, M. Characterization of Noncovalent Complexes of Antimalarial Agents of the Artemisinin-Type and Fe(III)-Heme by Electrospray Mass Spectrometry and Collisional Activation Tandem Mass Spectrometry. *J. Am. Soc. Mass Spectrom.* **2004**, *15*, 1181−1190.
(21) Jellen, E. E.; Ryzhov, V. Probing the Stability and Structure of Metalloporphyrin Complexes with Basic Peptides by Mass Spectrometry. *Eur. J. Mass Spectrom.* **2005**, *11*, 65−72.
(22) Siu, C. K.; Guo, Y.; Hopkinson, A. C.; Siu, K. W. How Large Is the $[Fe(III)(Protoporphyrin\ IX)]^+$ Ion ($Hemin^+$) in the Gas-Phase? *J. Phys. Chem. B* **2006**, *110*, 24207−24211.
(23) Duncan, M. A. Infrared Laser Spectroscopy of Mass-Selected Carbocations. *J. Phys. Chem. A* **2012**, *116*, 11477−11491.
(24) Polfer, N. C. Infrared Multiple Photon Dissociation Spectroscopy of Trapped Ions. *Chem. Soc. Rev.* **2011**, *40*, 2211−2221.
(25) Roithova, J. Characterization of Reaction Intermediates by Ion Spectroscopy. *Chem. Soc. Rev.* **2012**, *41*, 547−559.
(26) Baer, T.; Dunbar, R. C. Ion Spectroscopy: Where Did It Come from; Where Is It Now; and Where Is It Going? *J. Am. Soc. Mass Spectrom.* **2010**, *21*, 681−693.
(27) Fridgen, T. D. Infrared Consequence Spectroscopy of Gaseous Protonated and Metal Ion Cationized Complexes. *Mass Spectrom. Rev.* **2009**, *28*, 586−607.
(28) Eyler, J. R. Infrared Multiple Photon Dissociation Spectroscopy of Ions in Penning Traps. *Mass. Spectrom. Rev.* **2009**, *28*, 448−467.
(29) MacAleese, L.; Maitre, P. Infrared Spectroscopy of Organometallic Ions in the Gas-Phase: From Model to Real World Complexes. *Mass Spectrom. Rev.* **2007**, *26*, 583−605.
(30) Lanucara, F.; Scuderi, D.; Chiavarino, B.; Fornarini, S.; Maitre, P.; Crestoni, M. E. IR Signature of NO Binding to a Ferrous Heme Center. *J. Phys. Chem. Lett.* **2013**, *4*, 2414−2417.
(31) Chiavarino, B.; Crestoni, M. E.; Fornarini, S.; Lanucara, F.; Lemaire, J.; Maitre, P.; Scuderi, D. Direct Probe of NO Vibration in the Naked Ferric Heme Nitrosyl Complex. *ChemPhysChem* **2008**, *9*, 826−828.
(32) Lanucara, F.; Chiavarino, B.; Crestoni, M. E.; Scuderi, D.; Sinha, R. K.; Maitre, P.; Fornarini, S. Naked Five-Coordinate Fe(III)(NO) Porphyrin Complexes: Vibrational and Reactivity Features. *Inorg. Chem.* **2011**, *50*, 4445−4452.
(33) Chiavarino, B.; Maitre, P.; Fornarini, S.; Crestoni, M. E. Cynide-Arene Meisenheimer Complex Generated in Electrospray Ionization Mass Spectrometry Using Acetonitrile as a Solvent. *J. Am. Soc. Mass Spectrom.* **2013**, *24*, 1603−1607.
(34) Chiavarino, B.; Crestoni, M. E.; Maitre, P.; Fornarini, S. Halide Adducts of 1,3,5-Trinitrobenzene: Vibrational Signatures and Role of Anion-π Interactions. *Int. J. Mass Spectrom.* **2013**, *354*, 62−69.
(35) Chiavarino, B.; Crestoni, M. E.; Fornarini, S.; Lanucara, F.; Lemaire, J.; Maitre, P.; Scuderi, D. Molecular Complexes of Simple Anions with Electron-Deficient Arenes: Spectroscopic Evidence for Two Types of Structural Motifs for Anion-Arene Interactions. *Chem.—Eur. J.* **2009**, *15*, 8185−8195.
(36) Chiavarino, B.; Crestoni, M. E.; Fornarini, S.; Lanucara, F.; Lemaire, J.; Maitre, P. Meisenheimer Complexes Positively Characterized as Stable Intermediates in the Gas-Phase. *Angew. Chem., Int. Ed.* **2007**, *46*, 1995−1998.
(37) Crestoni, M. E.; Chiavarino, B.; Steinmetz, V.; Fornarini, S. Vibrational Study of a Benzyl Carbanion: Deprotonated 2,4-dinitrotoluene. *J. Chem. Phys.* **2012**, *137*, 181101/1−181101/4.
(38) De Petris, A.; Ciavardini, A.; Coletti, C.; Re, N.; Chiavarino, B.; Crestoni, M. E.; Fornarini, S. Vibrational Signatures of the Naked Aqua Complexes from Platinum(II) Anticancer Drugs. *J. Phys. Chem. Lett.* **2013**, *4*, 3631−3635.
(39) Chiavarino, B.; Crestoni, M. E.; Fornarini, S.; Scuderi, D.; Salpin, J. Y. Interaction of Cisplatin with Adenine and Guanine: A Combined IRMPD, MS/MS, and Theoretical Study. *J. Am. Chem. Soc.* **2013**, *135*, 1445−1455.
(40) Chiavarino, B.; Crestoni, M. E.; Fornarini, S.; Taioli, S.; Mancini, I.; Tosi, P. Infrared Spectroscopy of Copper-Resveratrol Complexes: A Joint Experimental and Theoretical Study. *J. Chem. Phys.* **2012**, *137*, 024307/1−9.
(41) Bakker, J. M.; Besson, T.; Lemaire, J.; Scuderi, D.; Maitre, P. Gas-Phase Structure of a π-Allyl-Palladium Complex: Efficient Infrared Spectroscopy in a 7 T Fourier Transform Mass Spectrometer. *J. Phys. Chem. A* **2007**, *111*, 13415−13424.
(42) Lemaire, J.; Boissel, P.; Heninger, M.; Mauclaire, G.; Bellec, G.; Mestdagh, H.; Simon, A.; Le Caer, S.; Ortega, J. M.; Glotin, F.; Maitre, P. Gas-Phase Infrared Spectroscopy of Selectively Prepared Ions. *Phys. Rev. Lett.* **2002**, *89*, 273002/1−4.
(43) Frisch, M. J.; Trucks, G. W.; Schlegel, H. B.; Scuseria, G. E.; Robb, M. A.; Cheeseman, J. R.; Scalmani, G.; Barone, V.; Mennucci, B.; Petersson, G. A.; et al. *Gaussian 09*, revision D.01; Gaussian, Inc.: Wallington, CT, 2009.
(44) de Visser, S. P.; Quesne, M. G.; Martin, B.; Comba, P.; Ryde, U. Computational Modelling of Oxygenation Processes in Enzymes and Biomimetic Model Complexes. *Chem. Commun.* **2014**, *50*, 262−282.
(45) Wondimagegn, T.; Rauk, A. The Structures and Stabilities of the Complexes of Biologically Available Ligands with Fe(III)-Porphine: An Ab Initio Study. *J. Phys. Chem. B* **2011**, *115*, 569−579.
(46) Swart, M. A Change in the Oxidation State of Iron: Scandium Is Not Innocent. *Chem. Commun.* **2013**, *49*, 6650−6652.
(47) Swart, M. Accurate Spin-State Energies for Iron Complexes. *J. Chem. Theory Comput.* **2008**, *4*, 2057−2066.
(48) Poater, A.; Vummaleti, S. V. C.; Cavallo, L. The "Innocent" Role of Sc^{3+} on a Non-heme Fe Catalyst in an O_2 Environment. *Dalton Trans.* **2014**, *43*, 11190−11194.
(49) Zvereva, E. E.; Shagidullin, A. R.; Katsyuba, S. A. Ab Initio and DFT Predictions of Infrared Intensities and Raman Activities. *J. Phys. Chem. A* **2011**, *115*, 63−69.
(50) Lykkegaard, M. K.; Zettergren, H.; Kirketerp, M. B.; Ehlerding, A.; Wyer, J. A.; Kadhane, U.; Brondsted Nielsen, S. Photodissociation of Isolated Ferric Heme and Heme-His Cations in an Electrostatic Ion Storage Ring. *J. Phys. Chem. A* **2009**, *113*, 1440−1444.
(51) Vaden, T. D.; de Boer, T. S.; MacLeod, N. A.; Marzluff, E. M.; Simons, J. P.; Snoek, L. C. Infrared Spectroscopy and Structure of Photochemically Protonated Biomolecules in the Gas-Phase: A Noradrenaline Analogue, Lysine and Alanyl Alanine. *Phys. Chem. Chem. Phys.* **2007**, *9*, 2549−2555.
(52) Adesokan, A. A.; Chaban, G. M.; Dopfer, O.; Gerber, R. B. Vibrational Spectroscopy of Protonated Imidazole and its Complexes with Water Molecules: Ab Initio Anharmonic Calculations and Experiments. *J. Phys. Chem. A* **2007**, *111*, 7374−7381.
(53) Sinha, R. K.; Nicol, E.; Steinmetz, V.; Maitre, P. Gas-Phase Structure of Micro-Hydrated $[Mn(ClO_4)]^+$ and $[Mn_2(ClO_4)_3]^+$ Ions Probed by Infrared Spectroscopy. *J. Am. Soc. Mass Spectrom.* **2010**, *21*, 758−772.
(54) Chiavarino, B.; Crestoni, M. E.; Fornarini, S.; Rovira, C. Protonated Heme. *Chem.—Eur. J.* **2007**, *13*, 776−785.
(55) Andriani, G.; Amata, E.; Beatty, J.; Clements, Z.; Coffey, B. J.; Courtemanche, G.; Devine, W.; Erath, J.; Juda, C. E.; Wawrzak, Z.; et al. Antitrypanosomal Lead Discovery: Identification of a Ligand-Efficient Inhibitor of *Trypanosoma Cruzi* CYP51 and Parasite Growth. *J. Med. Chem.* **2013**, *56*, 2556−2567.
(56) Egli, M.; Gessner, R. V. Stereoelectronic Effects of Deoxyribose O4′ on DNA Conformation. *Proc. Natl. Acad. Sci. U.S.A.* **1995**, *92*, 180−184.
(57) Wahl, M. C.; Sundaralingam, M. C−H···O Hydrogen Bonding in Biology. *Trends Biochem. Sci.* **1997**, *22*, 97−102.
(58) Simon, K.; Xu, J.; Kim, C.; Skrynnikov, N. R. Estimating the Accuracy of Protein Structures Using Residual Dipolar Couplings. *J. Biomol. NMR* **2005**, *33*, 83−93.
(59) Franzen, S. Effect of a Charge Relay on the Vibrational Frequencies of Carbonmonoxy Iron Porphine Adducts: The Coupling of Changes in Axial Ligand Bond Strength and Porphine Core Size. *J. Am. Chem. Soc.* **2001**, *123*, 12578−12589.
(60) Rydberg, P.; Sigfridsson, E.; Ryde, U. On the Role of the Axial Ligand in Heme Proteins: A Theoretical Study. *J. Biol. Inorg. Chem.* **2004**, *9*, 203−223.

DOI: 10.1021/jp5113476
J. Phys. Chem. B 2015, 119, 1919−1929

(61) Mishra, E.; Worlinsky, J. L.; Gilbert, T. M.; Bruckner, C.; Ryzhov, V. Axial Imidazole Binding Strengths in Porphyrinoid Cobalt(III) Complexes as Studied by Tandem Mass Spectrometry. *J. Am. Soc. Mass Spectrom.* **2012**, *23*, 1135−1146.
(62) Faria, J. L. B.; Almeida, F. M.; Pilla, O.; Rossi, F.; Sasaki, J. M.; Melo, F. E. A.; Mendes Filho, J.; Freire, P. T. C. Raman Spectra of L-Histidine Hydrochloride Monohydrate Crystal. *J. Raman Spectrosc.* **2004**, *35*, 242−248.
(63) Prell, J. S.; O'Brien, J. T.; Steill, J. D.; Oomens, J.; Williams, E. R. Structures of Protonated Dipeptides: The Role of Arginine in Stabilizing Salt Bridges. *J. Am. Chem. Soc.* **2009**, *131*, 11442−11449.
(64) Rajabi, K.; Fridgen, T. D. Structures of Aliphatic Amino Acid Proton-Bound Dimers by Infrared Multiple Photon Dissociation Spectroscopy in the 700−2000 cm^{-1} Region. *J. Phys. Chem. A* **2008**, *112*, 23−30.
(65) Chiavarino, B.; Crestoni, M. E.; Schutz, M.; Bouchet, A.; Piccirillo, S.; Steinmetz, V.; Dopfer, O.; Fornarini, S. Cation-π Interactions in Protonated Phenylalkylamines. *J. Phys. Chem. A* **2014**, *118*, 7130−7138.
(66) Roscioli, J. R.; McCunn, L. R.; Johnson, M. A. Quantum Structure of the Intermolecular Proton Bond. *Science* **2007**, *316*, 249−254.
(67) Durand, S.; Rossa, M.; Hernandez, O.; Paizs, B.; Maitre, P. IR Spectroscopy of B4 Fragment Ions of Protonated Pentapeptides in the X−H (X = C, N, O) Region. *J. Phys. Chem. A* **2013**, *117*, 2508−2516.

DOI: 10.1021/jp5113476
J. Phys. Chem. B 2015, 119, 1919−1929